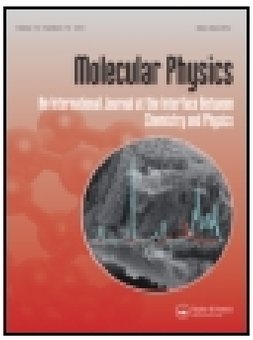

Taylor & Francis
Taylor & Francis Group

Molecular Physics

An International Journal at the Interface Between Chemistry and Physics

ISSN: 0026-8976 (Print) 1362-3028 (Online) Journal homepage: http://www.tandfonline.com/loi/tmph20

Solid-state NMR for bacterial biofilms

Courtney Reichhardt & Lynette Cegelski

To cite this article: Courtney Reichhardt & Lynette Cegelski (2014) Solid-state NMR for bacterial biofilms, Molecular Physics, 112:7, 887-894, DOI: 10.1080/00268976.2013.837983

To link to this article: http://dx.doi.org/10.1080/00268976.2013.837983

Accepted author version posted online: 02 Sep 2013.
Published online: 03 Oct 2013.

Molecular Physics, 2014
Vol. 112, No. 7, 887–894, http://dx.doi.org/10.1080/00268976.2013.837983

NEW VIEWS

Solid-state NMR for bacterial biofilms

Courtney Reichhardt and Lynette Cegelski*

Department of Chemistry, Stanford University, Stanford, CA, USA

(*Received 18 June 2013; accepted 19 August 2013*)

Bacteria associate with surfaces and one another by elaborating an extracellular matrix to encapsulate cells, creating communities termed biofilms. Biofilms are beneficial in some ecological niches, but also contribute to the pathogenesis of serious and chronic infectious diseases. New approaches and quantitative measurements are needed to define the composition and architecture of bacterial biofilms to help drive the development of strategies to interfere with biofilm assembly. Solid-state nuclear magnetic resonance (NMR) is uniquely suited to the examination of insoluble and complex macromolecular and whole-cell systems. This article highlights three examples that implement solid-state NMR to deliver insights into bacterial biofilm composition and changes in cell-wall composition as cells transition to the biofilm lifestyle. Most recently, solid-state NMR measurements provided a total accounting of the protein and polysaccharide components in the extracellular matrix of an *Escherichia coli* biofilm and transformed our qualitative descriptions of matrix composition into chemical parameters that permit quantitative comparisons among samples. We present additional data for whole biofilm samples (cells plus the extracellular matrix) that complement matrix-only analyses. The study of bacterial biofilms by solid-state NMR is an exciting avenue ripe with many opportunities and we close the article by articulating some outstanding questions and future directions in this area.

Keywords: biofilms; solid-state NMR; CPMAS; REDOR; bacterial cell walls

Introduction

Bacteria are ubiquitous across nature and have evolved an arsenal of survival techniques that enable them to colonise and even thrive in an astonishing range of environments, including those with extreme temperature and pH [1,2]. An important survival mechanism in niches ranging from within the human host to the extremely acidic microbial mats in Yellowstone is the cohabitation of bacteria in multicellular communities termed biofilms. Biofilms are composed of bacteria encased within a self-produced, non-crystalline extracellular matrix (ECM) that can consist of proteins, polysaccharides, lipids, and other molecules. Although bacteria have traditionally been studied as planktonic organisms, it is now appreciated that the majority of bacteria exist and persist as biofilms in nature [1]. Biofilms provide protection to bacteria through physical, chemical, and physiological mechanisms. The ECM can serve as a physical barrier against assaults such as ultraviolet light and chemical and biological antibacterial agents. The biofilm also harbours persister cells, or populations of dormant bacteria that are not responsive to antibiotics [3]. Although bacterial biofilms are essential for ecological stability in diverse niches on our planet, biofilm formation is also implicated in a number of adverse consequences, including aquatic biofouling [4]; contamination of medical devices [2,3] such as intravenous catheters, prosthetic heart valves, and artificial joints; and chronic bacterial infection [2,5].

Extensive research efforts to better understand biofilms have revealed their complexity and built an extensive foundation of measured parameters that aid in connecting biofilm properties with function [6]. These include the identification of genetic and molecular features that mediate and influence biofilm formation, patterns of nutrient flow within biofilm networks, and surface and mechanical properties of biofilm. However, biofilms pose a challenge to quantitative analysis by traditional biochemical techniques due to their insolubility and intractability [7]. Thus, while we have a basic parts list for some biofilms, including required molecular components, a complete accounting of the parts or atomistic structural detail of intact material has been lacking. New approaches are needed to transform biofilm descriptors into quantitative parameters of chemical and molecular composition. Some studies have employed Fourier transform infrared spectroscopy and solid-state nuclear magnetic resonance (NMR) to generally profile the types of chemical functionalities in biofilm samples, for example, carbonyls and peptide bonds, aromatics, and aliphatics [8–10]. Within this article, we describe the unique ability to implement solid-state NMR approaches to deliver quantitative insights regarding composition and structure in biofilm systems. At the close of this article, we discuss some of the exciting and promising future avenues utilising solid-state NMR to map the composition and structure of bacterial biofilms.

*Corresponding author. Email: cegelski@stanford.edu

Solid-state NMR for biological macrosystems

The cross-polarisation magic-angle spinning platform

Solid-state NMR is uniquely suited to the study of complex and insoluble systems such as bacterial biofilms [11–14]. It does not require homogeneous protein preparations or high-quality crystals (X-ray crystallography), high tumbling rates in solution (solution NMR), chemical processing, or enzymatic digestion (high pressure liquid chromatography-mass spectrometry (HPLC-MS)). Thus, solid-state NMR has been utilised to define composition, structure, and metabolism in a variety of otherwise intractable biological systems including bacterial whole cells and cell walls [15–18], amyloids [19–21], membrane proteins [22], and intact plant leaves [23,24]. Obtaining NMR spectra of such large and insoluble systems is not possible in solution-state NMR as the influence of dipolar couplings and chemical shift anisotropy (CSA) are not averaged out as they are in smaller, soluble, rapidly tumbling systems. Implementation of magic-angle spinning (MAS) in solid-state NMR experiments averages over the spatial coordinates in the dipolar coupling and CSA Hamiltonians and permits the acquisition of high-resolution spectra in solids [25–28]. Expressions for both Hamiltonians contain an angular dependence, $3\cos^2\theta - 1$, where θ is the angle between the internuclear spin vector and the external magnetic field. Thus, by mechanically spinning the sample at the magic angle ($\sim$54.74°), the '$3\cos^2\theta - 1$' term is averaged to zero and suppresses the influence of the dipolar coupling and CSA, yielding high-resolution NMR spectra harbouring the isotropic chemical shifts plus associated spinning sidebands [26,28]. A significant difference between MAS in solid-state NMR and molecular tumbling in solution-state NMR is that the spatial averaging is performed in a coherent manner, at a precise angle and frequency. Thus, since the dipolar coupling Hamiltonian, for example, depends on both space and spin coordinates, it is possible to manipulate the spin coordinates, interfere with the averaging, and extract the dipolar coupling (as in the rotational-echo double-resonance (REDOR) experiment [29]). In standard solution-state NMR experiments, the dipolar couplings are inaccessible unless the molecules are prepared in ways to induce alignment or enhance viscosity to restrict isotropic tumbling [30].

In most biological solids applications, MAS [25–28] is coupled with cross-polarisation (CP) [31–33] to enhance the NMR signal of nuclei with a low gyromagnetic ratio ($\gamma_{^{13}C} \approx \gamma_{^{1}H}/4$) by magnetisation transfer from ^{1}H nuclei by adjusting the radio frequency pulse power to satisfy Hartmann–Hahn matching conditions. The resulting cross-polarisation magic-angle spinning (CPMAS) experiment [34] is the platform for most biological solid-state NMR studies. Typical experiments employing CPMAS at low-to-modest spinning speeds (up to 15 kHz) are also performed in the presence of high-power proton decoupling to effect rapid spin flips among the ^{1}H nuclei to remove their couplings to other nuclei. These couplings can be reintroduced, if desired, by interrupted decoupling, for example, to distinguish between protonated and non-protonated carbons [35] or to estimate distances by spin diffusion [36].

Solid-state NMR insights into bacterial biofilm composition

Amyloid-integrated biofilm formation in Escherichia coli

We recently reported the first determination of the chemical composition of the intact ECM of a bacterial biofilm using solid-state NMR, biochemical analysis, and electron microscopy [37]. The NMR data provided the key quantitative parameters of the intact matrix – the percentages of matrix components by mass. The analysis was performed on an important human pathogenic bacterium, the uropathogenic *Escherichia coli* (UPEC) strain UTI89. As introduced earlier, this work was motivated by the need for fundamental chemical and molecular descriptions of bacterial biofilms in order to develop effective strategies to prevent and treat biofilm-associated infections. Biofilms are implicated in urinary tract infection (UTI), which most often is caused by UPEC [38,39]. UPEC can form biofilm-like intracellular bacterial communities [39] that evade host defences and antibiotic treatment, and are implicated in recurrent and persistent infections, including those associated with catheter-associated UTI [40]. We employed the UPEC strain, UTI89, which is a prototypical clinical isolate used in most of the pioneering *in vivo* work demonstrating the coordinated genetic and molecular cascade that accompanies host–pathogen interactions during infections of the bladder and kidneys [41–43]. UTI89 is also one of many *E. coli* clinical isolates that produce functional amyloid fibres termed curli [44,45]. Curli mediate adhesion to biotic and abiotic surfaces and, together with cellulose, serve as adhesive scaffolds and promote biofilm formation [46]. Although genetic and molecular analyses have determined that curli and cellulose, for example, can be co-produced in *E. coli* biofilms, the extent to which each one is present in the ECM had not been determined before the NMR work reviewed below [47–52]. Indeed, the general quantification of protein-to-polysaccharide ratios is difficult to determine by conventional analytical methods due to the resistance of the matrix to dissolution methods and the perturbation that accompanies harsh degradative methods to analyse biofilm parts.

Quantitative determination of the composition of the extracellular matrix in Escherichia coli

To define the protein and polysaccharide contributions to the biofilm framework, we obtained electron micrographs,

protein gels, and ^{13}C CPMAS spectra of (1) the complete ECM, (2) the curli-free ECM produced by the curli mutant strain UTI89Δ*csgA*, and (3) purified curli. These spectra indicated that the biofilm matrix formed by curli-producing bacteria has two major components, curli and cellulose, each in a quantifiable amount. The bacteria were grown on yeast extract plus casamino acids (YESCA) nutrient agar, a medium on which UTI89 exhibits the hallmark wrinkled colony morphology that is associated with *E. coli* biofilm production [47]. Congo red is often used in microbiological assays to enhance visualisation of this morphology [47], and growing the cells in the presence of this dye allowed us to visually track the presence of the ECM during the purification and to then precipitate the polysaccharide component of the ECM [37]. The non-perturbative purification procedure was based on the curli isolation protocol utilising fluid shear forces to remove the ECM while leaving the cells intact and separable by low-speed centrifugation [45].

The natural abundance of curli-only ^{13}C spectrum harbours contributions from all of its amino acids and differs from the carbon spectrum that would be associated with proteins with different amino acid sequences (Figure 1(A), top). Backbone and sidechain carbonyls contribute to the region around 175 ppm. Aromatic amino acid sidechains and also histidine and arginine sidechain carbons contribute to the region from 120 to 160 ppm, and the aliphatic region from 10 to70 ppm contains alpha carbons and other sidechain carbons. Each protein's unique pool of carbons based on the protein composition can be profiled in this way by one-dimensional CPMAS. The spectrum of UTI89Δ*csgA* ECM lacked a carbonyl peak, which indicated that there was no detectable protein in this sample (Figure 1(A), top). Instead, the UTI89Δ*csgA* spectrum contained contributions from both cellulose and Congo red, which were consistent with spectra of commercial cellulose and Congo red with the exception of an additional carbon peak at 40 ppm [37]. The 40-ppm carbon was hypothesised to be bonded to nitrogen, based on its chemical shift and the presence of a single nitrogen amine peak in the ^{15}N CPMAS spectrum of a uniform ^{15}N biosynthetically labelled sample for which cells were grown in the presence of $^{15}NH_4Cl$. This possibility was investigated by $^{13}C\{^{15}N\}$ REDOR, a solid-state NMR experiment that enables the measurement of heteronuclear dipolar couplings between heteronuclear spin pairs in a sample [12,13,29]. In this case, a one-bond $^{13}C\{^{15}N\}$ REDOR filter revealed that the 40-ppm carbon was completely dephased and was directly bonded to a nitrogen. Together with the collective chemical shifts, the 40-ppm carbon was determined to be consistent with a hydroxyl-substituted, O-linked 2-aminoethyl modification of cellulose [37,53–55]. By deconvolution of the ^{13}C CPMAS spectra, the UTI89Δ*csgA* sample was determined to contain 50% Congo red and 50% of the modified cellulose [37]. The wild-type UTI89 spectrum was

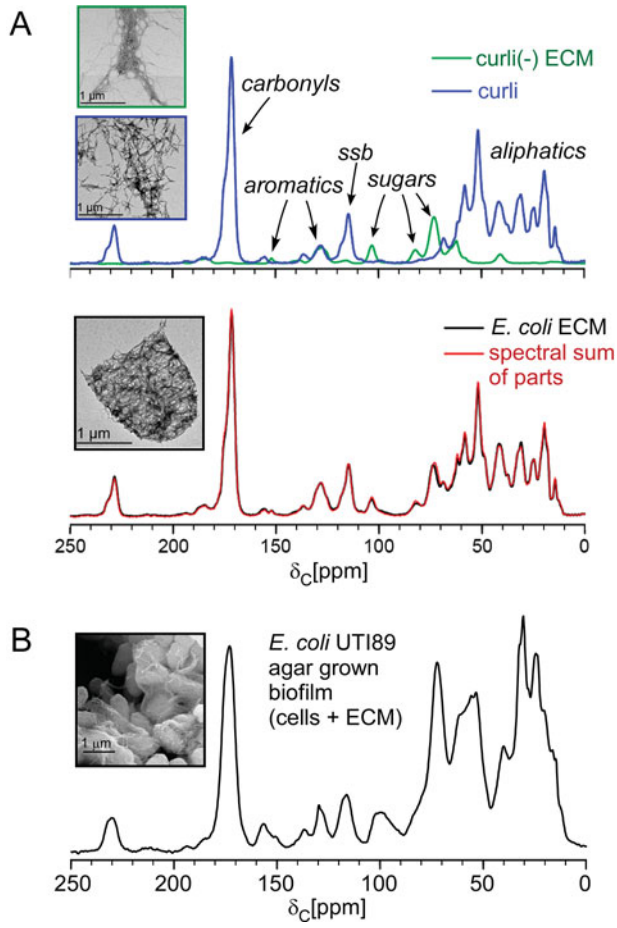

Figure 1. NMR sum of the parts. (A) The spectral sum of the UTI89Δ*csgA* extracellular material and purified curli (top) completely recapitulates the ^{13}C CPMAS spectrum of the intact UTI89 ECM (bottom), each associated with transmission electron micrographs associated with the samples. MAS was performed at 7143 Hz and 32,768 scans were obtained for each spectrum. (B) The ^{13}C CPMAS spectrum of the whole biofilm sample contains carbon contributions from whole cells plus the ECM. MAS was performed at 7143 Hz. This figure is adapted from reference [37], with permission from Elsevier.

a nearly perfect match for the spectral sum of the scaled spectra of the curli and UTI89Δ*csgA* ECM (Figure 1(A), bottom). The scaled sum was obtained by normalising each spectrum by its mass and scaling the curli spectrum to 72% and the UTI89Δ*csgA* to 28%. After accounting for the Congo red in the UTI89Δ*csgA* sample, we found that the UTI89-insoluble ECM grown on the YESCA nutrient agar was composed of a 6:1 ratio of curli to polysaccharide. This result was further confirmed by obtaining the ^{13}C CPMAS spectrum of a physical mixture of biofilm parts within one rotor [37] and has provided the first total accounting of the components of the intact ECM of a bacterial biofilm.

Previous biochemical studies that have examined the general production of curli have only profiled whether curli

production is either increased or decreased relative to a reference sample as a function of bacterial strain or environmental conditions. These analyses do not provide an absolute concentration or the relative amount of curli with respect to other components. Some reviews assume that extracellular matrices would be primarily polysaccharide [56] (due to the appreciated 'stickiness' of polysaccharides), perhaps 80% polysaccharide and 20% curli in the case of *E. coli*. Thus, the development of this approach *and* the determination that the insoluble matrix is 85% curli and 15% polysaccharide in the specified growth conditions are the first determination of the composition of an ECM and provide a valuable first-of-kind strategy that can be recruited to answer many exciting questions regarding other biofilm formers and the influence of biofilm inhibitors.

Mapping of global carbon pools in the intact biofilm by solid-state NMR

Comparison of the ^{13}C CPMAS spectrum of the intact biofilm, including the bacterial whole cells plus the ECM, is also provided here in Figure 1(B). There is an increased number of carbon contributions, as expected, from the cellular contents, including the abundant diversity of macromolecules, for example, proteins and nucleic acids, as well as lipids, carbohydrates, metabolites, and small molecules. The spectrum harbours broad resonances that represent the vast array of chemical environments represented in the whole cells. Indeed, most of the mass of the whole biofilm in these preparations arises from the intact cells. Thus, in the dissection of the composition of the ECM (Figure 1(A)), it was invaluable to be able to extract the ECM from the biofilm for analysis by solid-state NMR. We employed a minimally perturbative method for extraction of the ECM from bacterial biofilms that relies upon homogenisation with shear force followed by differential centrifugation to separate the ECM from the bacterial cells, a procedure that is useful for the extraction of ECM from biofilms formed by other strains and species of bacteria, although the ECM of some organisms is difficult to extract and alternate protocols are developed as needed to permit their isolation.

NMR comparison of UTI89 carbon pools in intact biofilms at the air–liquid interface

As shown above, solid-state NMR has the sensitivity and resolution to profile the global carbon composition of intact biofilms containing cells plus the ECM. We utilised NMR to study the influence of the small molecule dimethyl sulphoxide (DMSO) on biofilm production, specifically biofilms formed at the air–liquid interface, referred to as pellicles [57]. *E. coli* exhibits a selective increase in curli protein expression (*csgA* and *csgB* mRNA expression increases over 10-fold) in response to DMSO, resulting in an increase in curli production (Figure 2(A)) and a visually observable

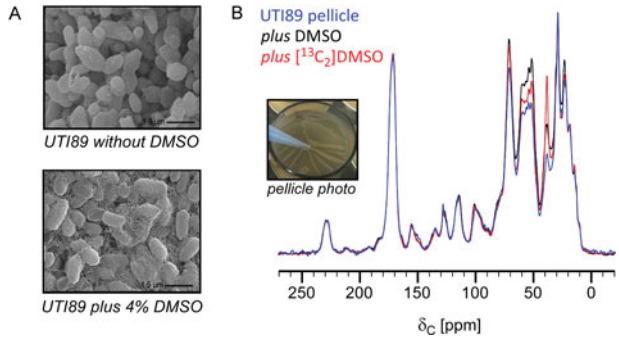

Figure 2. Comparative analysis of carbon pools in intact pellicles. (A) Transmission electron micrographs of pellicles formed in YESCA nutrient broth in the presence and absence of 4% DMSO. (B) Natural-abundance ^{13}C CPMAS NMR spectra provided a complete accounting of the carbon contributions in intact pellicles formed by UTI89 in the absence of DMSO and in the presence of DMSO and [$^{13}C_2$]DMSO. Treatment with DMSO increases curli production and is accompanied by a spectroscopic increase in carbons in the 50–75 ppm region, with respect to the carbonyl peak. Except for the enhancement in peak intensity at 39 ppm (the isotropic carbon chemical shift of DMSO), growth in medium supplemented with labelled [$^{13}C_2$]DMSO did not result in other carbon-peak intensity increases as compared to treatment with unlabelled DMSO. This figure is adapted from reference [57], with permission from the American Society for Microbiology.

increase in film robustness, an acceleration and increase in the development of the elastic modulus of the film, and an enhancement in the ability to recover from strain [57,58]. This effect is tunable as a function of DMSO concentration, ranging from 0.5% (*v*/*v*) to 4% (*v*/*v*). Given the relatively high concentration of DMSO in the nutrient broth, we examined whether the increases in curli production could be, in part, attributed to the utilisation of DMSO as a carbon source. Thus, ^{13}C CPMAS spectra of intact pellicles formed by UTI89 in the presence of DMSO or [$^{13}C_2$]DMSO were compared. If DMSO was used as a carbon source, an increase in peak intensity at a chemical shift corresponding to that of an end metabolic product in the [$^{13}C_2$]DMSO sample relative to that of the unlabelled DMSO growth conditions would have been observed. However, the only observable increase in peak intensity in the [$^{13}C_2$]DMSO sample appeared at 39 ppm, which corresponds to the DMSO carbon chemical shift resulting from residual [$^{13}C_2$]DMSO among the harvested cells (Figure 2(B), black and red) [57]. These results indicated that the enhancements in biofilm formation observed in the presence of DMSO were not connected to any utilisation of the DMSO as a carbon source, which would have led to overall increases in some carbon-peak intensities. Overall, the two spectra were similar, also revealing the biological similarity of different biofilm preparations. It has been our experience with other whole-cell and cell-wall systems that significant fluctuations in carbon pools are not observed among such preparations, which leads to the power in comparisons when using CPMAS to

examine complex bacterial systems. Here, we also include the non-DMSO-treated pellicle for comparison (Figure 2, blue). The three spectra were scaled according to the carbonyl peak to enable the detection of relative differences in the carbon pools. Treatment with DMSO did yield increases in the 50–75 ppm chemical-shift range relative to the carbonyl peak height as compared to the sample without DMSO treatment, and it presents a whole biofilm signature that is associated with increased curli and ECM production.

Biofilm formation in Gram-positive bacteria

Cell surfaces and biofilms in Staphylococcus aureus

Gram-positive bacteria, such as *Staphylococcus aureus*, differ from Gram-negative bacteria, such as *E. coli* and *Salmonella*, in their cellular organisation. Gram-negative bacteria harbour an inner membrane, a periplasmic space containing a thin layer of peptidoglycan, and an outer membrane. The ECM in Gram-negative bacteria is produced beyond the outer membrane and the ECM components must be secreted through the outer membrane. In contrast, Gram-positive bacteria harbour a single cell membrane surrounded by a thick layer of cell-wall material composed primarily of peptidoglycan. Biofilm formation by *S. aureus* is characterised by the production of an ECM outside its thick cell wall [59] and, like *E. coli*, biofilm-associated *S. aureus* infections are also a significant concern in the clinic [59,60]. We and others are beginning to study Gram-positive biofilm formation by solid-state NMR. We are interested in examining the *S. aureus* ECM framework and the variability in the ECM as a function of strain or external stimuli such as antibiotic treatment. En route to studying the *S. aureus* ECM, we recently discovered that the *S. aureus* peptidoglycan is altered as cells progress through the stationary phase, increasing in cell density and depleting nutrients from the growth medium [37]. We believe that considerations of cell-wall composition and architecture will be important in fully understanding biofilm formation in *S. aureus* and other Gram-positive bacteria. There is precedence for this notion, as peptidoglycan breaks have been identified in lactococcal biofilm communities and are correlated with the ability to form biofilms [61]. Bacteria that lacked the proper peptidoglycan hydrolase could not alter their cell wall and were deficient in adhesion and unable to form biofilms [61]. Biofilm formation was restored by the addition of exogenous hydrolases to perturb the cell wall [61]. Similarly, based on biochemical data and functional phenotypes, peptidoglycan remodelling has been implicated in adhesion and biofilm formation in *Pseudomonas aeruginosa* and *E. coli*, potentially to allow for proper assembly of large macromolecular complexes involved in adhesion and biofilm assembly [62]. Thus, we describe our recent discovery of significant cell-wall alterations in bacterial cultures as a function of cell density and nutrient limitation.

Cell-wall compositional changes in Staphylococcus aureus *during nutrient limitation in the stationary phase*

We have started to study the composition of the *S. aureus* ECM, but first made some discoveries regarding the cell-wall composition as cells reach the stationary phase and deplete nutrients from the surrounding medium, events that promote biofilm formation *in vivo* and in the laboratory [54]. Ultimately, one wants to map and understand all the changes in the biofilm community, those that occur within the individual cells (in the cytoplasm and in the cell wall) and those that occur in the ECM. Solid-state NMR has been used extensively, particularly over the past 10 years, to examine bacterial cell-wall composition and architecture in Gram-positive bacteria such as *S. aureus* and in defining the modes of action of cell-wall-targeting antibiotics [17,18,63–65], although these studies are beyond the scope of this perspective. The major component of the cell wall is the peptidoglycan [66]. The peptidoglycan is a mesh-like network consisting of polymerised peptidoglycan subunits that are synthesised inside the cell and transported to the cell surface for polymerisation via transglycosylation (linking of the sugars) and transpeptidation (linking of the peptide stems). In *S. aureus*, the peptidoglycan precursor consists of a disaccharide linked to a pentapeptide stem (L-Ala-D-isoglutamine-L-Lys-D-Ala-D-Ala) that is normally functionalised with a pentaglycine bridge attached to the ε-amino group of the L-Lys of the pentapeptide. During transpeptidation, the pentaglycine bridge becomes cross-linked to the penultimate D-Ala of a neighbouring stem, accompanied by the concomitant loss of the terminal D-Ala (Figure 3(A)). The highly cross-linked peptidoglycan of *S. aureus* cannot be fully digested by chemical or enzymatic hydrolysis and thus cannot be fully resolved by traditional biochemical techniques including HPLC-MS, emphasising the necessity of a method such as solid-state NMR to characterise the intact peptidoglycan.

Using ^{15}N CPMAS, we quantified populations of bridge links in a specifically labelled peptidoglycan across different growth stages as cells increase in density in the stationary phase [16]. Peptidoglycan was isolated from specifically L-[ε-^{15}N]Lys-labelled cells, where the L-[ε-^{15}N]Lys label does not scramble as evidenced by the lack of ^{15}N peaks corresponding to other amino acid sidechains [16]. In the exponential growth stage, only one peak was observed in the ^{15}N CPMAS spectrum (Figure 3(B)), assigned to the amide form of the Lys ε-N in a bridge link with the pentaglycine bridge attached (Figure 3(A)) [16]. In contrast, the spectrum of the peptidoglycan isolated from bacteria harvested in the stationary growth stage contained a second peak, which increased at later growth stages and was assigned to the amine form of the Lys ε-N, corresponding to stems without attached bridges. Interestingly, cell-wall septa were also thicker in the stationary phase (Figure 3(B)). The changes in nutrient levels in the broth medium during

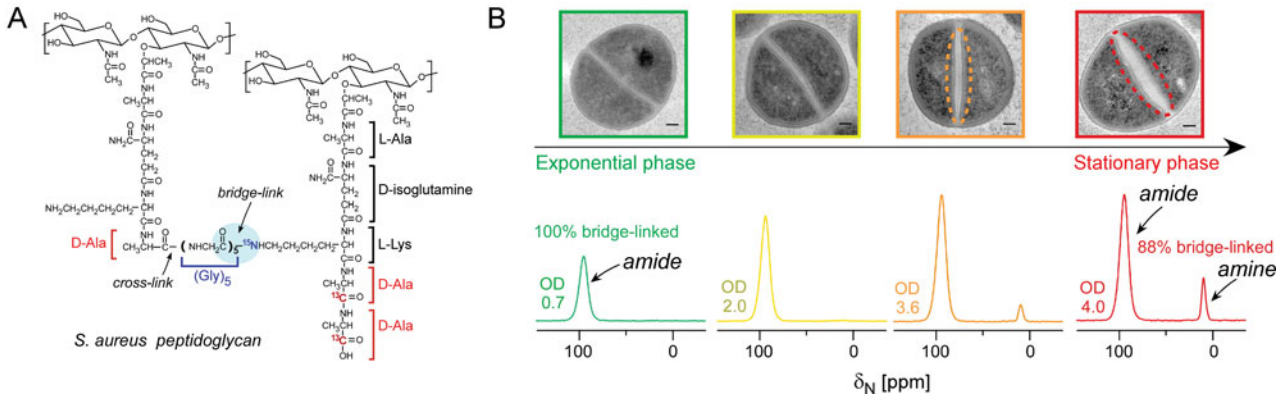

Figure 3. Alterations in the *S. aureus* cell wall during stationary phase and nutrient depletion. (A) Chemical structure of *S. aureus* peptidoglycan, which is cross-linked through an interpeptide bridge consisting of five glycines to connect the ε-amino group of L-Lys in the third position of one stem (bridge link, highlighted) to the D-Ala in the fourth position of the connected stem (cross-link) with the concomitant cleavage of the terminal D-Ala. (B, top) TEM images of ultrathin sections of *S. aureus* cells harvested at four different growth stages, where non-uniform thickening is indicated with dashed lines in the TEM images of cells harvested at optical density (OD) 3.6 and OD 4. Scale bars are 100 nm. (B, bottom) ^{15}N CPMAS spectra of [ε-^{15}N]Lys-labelled peptidoglycan isolated from *S. aureus* cells at OD 0.7, OD 2, OD 3.6, and OD 4. Spectra are normalised to the amide peak. The amine peak at 10 ppm appears at OD 2.0 (not obvious) and increases towards OD 4 (stationary phase). Spectra were acquired on a 500-MHz spectrometer with MAS at 8 kHz and were referenced to solid ammonium sulphate. This figure is adapted from reference [16], with permission from Zhou and Cegelski.

bacterial growth were monitored by solution NMR, and the emergence of the peptide stems without glycine bridges occurred concomitantly with the depletion of glycine from the nutrient medium [16]. Thus, the bacteria transported imperfect stems to the extracellular surface, rather than slowing down cell-wall synthesis until glycine production could increase and canonical cell-wall precursors could be assembled and transported to the cell surface for assembly. Pulse–chase labelling experiments confirmed that the emergence of peptidoglycan stems with the free lysyl amines resulted from new cell-wall synthesis rather than from the degradation of the existing cell wall. Future work will explore whether the decreased cross-linking provides an advantage to the bacteria, perhaps by allowing increased porosity to transport large proteins beyond the cell wall as they assemble biofilms or, alternatively, if the production of the altered and less highly cross-linked cell wall renders the cells more sensitive to antibiotics that target cell-wall assembly.

Conclusions and future avenues

We have recently launched solid-state NMR as a valuable approach to determine the composition of the bacterial ECM. We defined the composition of the *E. coli* ECM under amyloid-integrated biofilm growth conditions, transforming qualitative descriptions of the ECM into quantitative parameters based on molecular composition and spectroscopic signatures that can be compared across samples. Traditional forms of analyses have provided only qualitative identification of the components of biofilms without a quantitative understanding of their molecular connectivity and structural complexities. The understanding and methodology that we have developed will be valuable to the continued study of the fundamental chemical and molecular basis of biofilm structure involving a range of disciplines including (1) microbiology, especially as new bacterial amyloids are discovered and (2) structural biology and biophysics, similar to the study of other large macromolecular complexes and machinery including bacterial cell walls, flagella, and ATP synthase. Thus far, we have successfully described and provided an accounting for the components of the ECM of a clinically relevant *E. coli* strain UTI89. Previous studies of curli-integrated biofilms only profiled whether curli production was either increased or decreased. Thus, the development of the integrated approach summarised here *and* the determination that the matrix is 85% curli and 15% polysaccharide in the specified growth conditions provide a first-of-kind strategy that can be recruited to answer many exciting questions regarding other biofilm formers. Key insights can emerge from unlabelled samples with only natural-abundance carbon contributions. Thus, the approach is broadly applicable to examining biofilm production among other strains and species of bacteria, including organisms such as *S. aureus*, *Pseudomonas aeruginosa*, and *Vibrio cholerae*.

There are many fundamental questions about biofilm formation that remain unanswered and can begin to be explored with solid-state NMR. We can explore the types and extent of contacts that exist between the biofilm components and begin to create atomistic maps of biofilm structure. Indeed, it should be possible to utilise biosynthetic labelling strategies and NMR detection schemes beyond what we have discussed in this review to further refine our developing description of a biofilm and its corresponding ECM as an organised assembly of polymeric macromolecules,

connecting composition, structure, and function. The lessons learned from nature's assembly of biofilms may even inspire the synthesis of materials with new properties. Another significant opportunity and scientific need is to examine the influence of biofilm inhibitors [5,67]. The non-crystalline and insoluble nature of biofilms makes it difficult to determine the localisation of small molecules in biofilms using conventional methods. However, solid-state NMR can be used to map the binding of small molecules to biofilm components and to assess the changes in biofilm composition and structure, helping to reveal the molecular modes of action of biofilm inhibitors. This understanding can help to drive the development of new biofilm inhibitors needed to prevent undesired bacterial colonisation and biofilm formation associated with disease.

Acknowledgements

L. Cegelski holds a Career Award at the Scientific Interface from the Burroughs Welcome Fund. C. Reichhardt is the recipient of the Stanford Graduate Fellowship. We gratefully acknowledge support from the NIH Director's New Innovator Award, Stanford University, the Stanford Terman Fellowship, and the Hellman Faculty Scholar Award.

References

[1] L. Hall-Stoodley, J.W. Costerton, and P. Stoodley, Nat. Rev. Microbiol. **2** (2), 95–108 (2004).
[2] R.M. Donlan and J.W. Costerton, Clin. Microbiol. Rev. **15** (2), 167–193 (2002).
[3] J.L. del Pozo and R. Patel, Clin. Pharmacol. Ther. **82** (2), 204–209 (2007).
[4] H.C. Flemming, Appl. Microbiol. Biot. **59** (6), 629–640 (2002).
[5] L. Cegelski, G.R. Marshall, G.R. Eldridge, and S.J. Hultgren, Nat. Rev. Microbiol. **6** (1), 17–27 (2008).
[6] H.C. Flemming and J. Wingender, Nat. Rev. Microbiol. **8** (9), 623–633 (2010).
[7] I.W. Sutherland, Microbiol. UK **147**, 7 (2001).
[8] J. Ha, A. Gelabert, A.M. Spormann, and G.E. Brown, Geochim. Cosmochim. Acta **74** (1), 1–15 (2010).
[9] Y.Q. Jiao, G.D. Cody, A.K. Harding, P. Wilmes, M. Schrenk, K.E. Wheeler, J.F. Banfield, and M.P. Thelen, Appl. Environ. Microb. **76** (9), 2916–2922 (2010).
[10] J.Y. Lim, J.M. May, and L. Cegelski, Appl. Environ. Microb. **78** (9), 3369–3378 (2012).
[11] K.J. Kramer, T.L. Hopkins, and J. Schaefer, in *Nitrogen-Containing Macromolecules in the Bio- and Geosphere*, ACS Symposium Series, edited by B.A. Stankiewicz and P.F. van Bergen (American Chemical Society, Washington, DC, 1998), Vol. 707, pp. 14–33.
[12] S.L. Grage and A. Watts, in *Annual Reports on NMR Spectroscopy*, edited by G. Webb (Academic Press, San Diego, 2006), Vol. 60, pp. 191–228.
[13] T. Gullion, in *Annual Reports on NMR Spectroscopy*, edited by G. Webb (Academic Press, Oxford, 2009), Vol. 65, pp. 111–137.
[14] M. Renault, A. Cukkemane, and M. Baldus, Angew. Chem. Int. Edit. **49** (45), 8346–8357 (2010).
[15] O. Toke and L. Cegelski, in *Solid State NMR Studies of Biopolymers*, edited by A.E. McDermott and T. Polenova (Wiley, Chichester, 2010), pp. 473–490.
[16] X. Zhou and L. Cegelski, Biochem. **51** (41), 8143–8153 (2012).
[17] S.J. Kim, L. Cegelski, D.R. Sutdelska, R.D. O'Connor, A.K. Mehta, and J. Schaefer, Biochem. **41**, 6967 (2002).
[18] S.J. Kim, L. Cegelski, M. Preobrazhenskaya, and J. Schaefer, Biochem. **45**, 5235 (2006).
[19] R. Tycko, Q. Rev. Biophys. **39** (1), 1–55 (2006).
[20] R. Tycko, Ann. Rev. Phys. Chem. **62**, 279 (2011).
[21] A.T. Petkova, Y. Ishii, J.J. Balbach, O.N. Antzutkin, R.D. Leapman, F. Delaglio, and R. Tycko, Proc. Natl. Acad. Sci. USA **99** (26), 16742–16747 (2002).
[22] A. McDermott, Ann. Rev. Biophys. **38** (1), 385–403 (2009).
[23] L. Cegelski and J. Schaefer, J. Biol. Chem. **280** (47), 39238–39245 (2005).
[24] R.C. Dirks, M. Singh, G.S. Potter, L.G. Sobotka, and J. Schaefer, New Phytol. **196** (4), 1109–1121 (2012).
[25] E.R. Andrew, A. Bradbury, and R.G. Eades, Nature **182** (4650), 1659 (1958).
[26] E.R. Andrew and R.A. Newing, Proc. Phys. Soc. London **72** (468), 959–972 (1958).
[27] E.R. Andrew, A. Bradbury, and R.G. Eades, Nature **183** (4678), 1802–1803 (1959).
[28] I.J. Lowe, Phys. Rev. Lett. **2** (7), 285–287 (1959).
[29] T. Gullion and J. Schaefer, J. Magn. Reson. **81**, 196 (1989).
[30] J.H. Prestegard, H.M. Al-Hashimi, and J.R. Tolman, Q. Rev. Biophys. **33** (4), 371–424 (2000).
[31] S.R. Hartmann and E.L. Hahn, Phys. Rev. **128** (5), 2042–2053 (1962).
[32] F.M. Lurie and C.P. Slichter, Phys. Rev. A **133** (4A), 1108–1122 (1964).
[33] A. Pines, M.G. Gibby, and J.S. Waugh, J. Chem. Phys. **59** (2), 569–590 (1973).
[34] J. Schaefer and E.O. Stejskal, J. Am. Chem. Soc. **98** (4), 1031–1032 (1976).
[35] S.J. Opella and M.H. Frey, J. Am. Chem. Soc. **101** (19), 5854–5856 (1979).
[36] D.E. Demco, A. Johansson, and J. Tegenfeldt, Solid State Nucl. Mag. **4** (1), 13–38 (1995).
[37] O.A. McCrate, X. Zhou, C. Reichhardt, and L. Cegelski, J. Mol. Biol. (in press) <http://dx.doi.org/10.1016/j.jmb.2013.06.022>.
[38] G.G. Anderson, K.W. Dodson, T.M. Hooton, and S.J. Hultgren, Trends Microbiol. **12** (9), 424–430 (2004).
[39] G.G. Anderson, J.J. Palermo, J.D. Schilling, R. Roth, J. Heuser, and S.J. Hultgren, Science **301** (5629), 105–107 (2003).
[40] S.M. Soto, A. Smithson, J.A. Martinez, J.P. Horcajada, J. Mensa, and J. Vila, J. Urology **177** (1), 365–368 (2007).
[41] M.A. Mulvey, J.D. Schilling, and S.J. Hultgren, Infect. Immun. **69** (7), 4572–4579 (2001).
[42] S.S. Justice, C. Hung, J.A. Theriot, D.A. Fletcher, G.G. Anderson, M.J. Footer, and S.J. Hultgren, Proc. Natl. Acad. Sci. USA **101** (5), 1333–1338 (2004).
[43] G.G. Anderson, J.J. Palermo, J.D. Schilling, R. Roth, J. Heuser, and S.J. Hultgren, Science **301** (5629), 105–107 (2003).
[44] A. Olsen, A. Jonsson, and S. Normark, Nature **338** (6217), 652–655 (1989).
[45] M.R. Chapman, L.S. Robinson, J.S. Pinkner, R. Roth, J. Heuser, M. Hammar, S. Normark, and S.J. Hultgren, Science **295** (5556), 851–855 (2002).
[46] M.M. Barnhart and M.R. Chapman, Annu. Rev. Microbiol. **60**, 131 (2006).
[47] X. Zogaj, M. Nimtz, M. Rohde, W. Bokranz, and U. Romling, Mol. Microbiol. **39**, 1452 (2001).

[48] C. Beloin, A. Roux, and J.M. Ghigo, Curr. Top. Microbiol. Immunol. **322**, 249 (2008).
[49] X. Zogaj, W. Bokranz, M. Nimtz, and U. Romling, Infect. Immun. **71** (7), 4151–4158 (2003).
[50] S. Da Re and J.M. Ghigo, J. Bacteriol. **188** (8), 3073–3087 (2006).
[51] L. Gualdi, L. Tagliabue, S. Bertagnoli, T. Ierano, C. De Castro, and P. Landini, Microbiol. **154** (Pt 7), 2017–2024 (2008).
[52] Z. Saldana, J. Xicohtencatl-Cortes, F. Avelino, A.D. Phillips, J.B. Kaper, J.L. Puente, and J.A. Giron, Environ. Microbiol. **11** (4), 992–1006 (2009).
[53] A. Kai, P. Xu, F. Horii, and S.H. Hu, Polymer **35**, 75 (1994).
[54] S. Maunu, T. Liitia, S. Kauliomaki, B. Hortling, and J. Sundquist, Cellulose **7**, 147 (2000).
[55] T.K. Lindhorst, S. Kötter, U. Krallmann-Wenzel, and S. Ehlers, J. Chem. Soc. Perk. T **1** (8), 823–831 (2001).
[56] I.W. Sutherland, Trends in Microbiol. **9**, 222 (2001).
[57] J.Y. Lim, J.M. May, and L. Cegelski, Appl. Environ. Microb. **78** (9), 3369–3378 (2012).
[58] C. Wu, J.Y. Lim, G.G. Fuller, and L. Cegelski, Biophys. J. **103** (3), 464–471 (2012).
[59] M. Otto, Annu. Rev. Med. **64**, 175 (2013).
[60] M.R. Kiedrowski and A.R. Horswill, Ann. N.Y. Acad. Sci. **1241** (1), 104–121 (2011).
[61] C. Mercier, C. Durrieu, R. Briandet, E. Domakova, J. Tremblay, G. Buist, and S. Kulakauskas, Mol. Microbiol. **46** (1), 235–243 (2002).
[62] C.V. Gallant, C. Daniels, J.M. Leung, A.S. Ghosh, K.D. Young, L.P. Kotra, and L.L. Burrows, Mol. Microbiol. **58** (4), 1012–1024 (2005).
[63] L. Cegelski, S.J. Kim, A.W. Hing, D.R. Studelska, R.D. O'Connor, A.K. Mehta, and J. Schaefer, Biochem. **41**, 13053 (2002).
[64] S. Sharif, M. Singh, S.J. Kim, and J. Schaefer, J. Am. Chem. Soc. **131**, 7023 (2009).
[65] S.J. Kim, K.S.E. Tanaka, E. Dietrich, A.R. Far, and J. Schaefer, Biochem. **52** (20), 3405–3414 (2013).
[66] W. Vollmer, D. Blanot, and M.A. de Pedro, FEMS Microbiol. Rev. **32** (2), 149–167 (2008).
[67] L. Cegelski, J.S. Pinkner, N.D. Hammer, C.K. Cusumano, C.S. Hung, E. Chorell, V. Aberg, J.N. Walker, P.C. Seed, F. Almqvist, M.R. Chapman, and S.J. Hultgren, Nat. Chem. Biol. **5** (12), 913–919 (2009).